Impact of Weight Functions on Performance of Three-Input Integrated Dc-Dc Converter in H_∞ Control

MANOGNA M., AMARENDRA REDDY B., PADMA KOTTALA
Department of Electrical Engineering,
Andhra University College of Engineering,
Visakhapatnam, Andhra Pradesh,
INDIA

Abstract: - Many power electronic systems applications namely locomotives, hybrid electric vehicles, and all renewable energy sourced systems are shifting towards Multi-Input Multi-Output (MIMO) integrated DC-DC converters due to their reliability and flexible nature. Designing controllers for MIMO integrated DC-DC converter is complicated due to its integrated structure, presence of common elements, and interactions between the input and output variables of the converter. In this work, a Three-Input Integrated DC-DC (TIID) converter is modeled using state-space analysis, and a Transfer Function Matrix (TFM) is acquired from the small signal continuous time model. A robust H_∞ controller based on the loop shaping method is designed for the TIID converter. In this loop-shaping method, the desired robustness and the performance of the controller are represented with weight functions i.e., loop-shaping filters. These weight functions are designed using TFM and are frequency-dependent. The robustness of the controller depends on the weight function parameters. The effect of varying the parameters of the weight functions on system dynamics, robustness, and performance are studied and plotted. TIID converter of 288 W, 24V-30V-36V to 48 V is considered and the impact of weight function on closed-loop system dynamics and sensitivity characteristics under varying parameter conditions are analyzed in MATLAB Environment.

Key-Words: - Three-Input Integrated Dc-dc (TIID) converter, state-space modeling, small-signal analysis, Transfer Function Matrix (TFM), Weight Function Matrix (WFM), H_∞ controller.

Received: March 15, 2023. Revised: January 6, 2024. Accepted: March 7, 2024. Published: April 11, 2024.

1 Introduction

The MIMO converters are proven to be more flexible, efficient, reliable, and economical, [1], [2], [3], [4], in many power electronic systems applications namely locomotives, hybrid electric vehicles, and all renewable energy-sourced systems. Thus, designing a MIMO PID controller is more complicated than a Single-Input Single-Output (SISO) PID controller. Since the number of tuning parameters is limited to three in the SISO case, the problem of designing a SISO PID is rather simple and a wide variety of methods are available for this purpose, [5], [6].

Different methodologies to design MIMO PID controllers for MIMO systems that ensure stability and performance are reported in the recent literature, [7], [8]. Diagonal controllers are proposed for a Two-input Buck-SEPIC dc-dc converter system using individual channel design (ICAD), [9]. A decoupler network is designed to minimize the control-loop interactions for a three-port dc-dc converter which is suitable for a satellite application, [10]. The interaction -independent robust controller is designed for a two-input fourth-order integrated (TIFOI) dc-dc converter, [11], using H_∞ Loop Shaping design procedure. H_∞ loop-shaping controllers are extensively studied and applied to a MIC, [12]. According to H_∞ control, [13], the infinity norm of the closed-loop system is minimized in designing a controller which is related to the robust stability margin of the closed-loop system. The advantage of a H_∞ controller over other controllers is that it can be directly used to handle single-input as well as multi-input systems with cross-coupling between channels, [14], [15].

The controller design using an H_∞ loop-shaping procedure is proposed for a MIMO system and presented in [16], [17] and [18]. Robust controller design through the H∞ loop-shaping method is extensively studied and applied to a MIC, [19]. Here, the robustness of a closed-loop system is ensured by the controller designed using a loop-shaping technique. Weight function formulation is difficult for MIMO systems because each input signal may affect many controlled variable output signals. It is important to study the impact of interactions between inputs and outputs beforehand.

Novelty/ Contribution of the work:

In this work, a systematic way of identifying the weight functions for TIID converter using H_∞ methods is presented. According to H_∞ control theory, [20], [21], [22], the infinity norm of the weighted sensitivity function is minimized in controller design, and infinity norm is related to the robust stability margin of the closed-loop system. The following contributions are made from this work:

(i) A fourth-order TIID converter is proposed in [23]. Here, the guidelines from [24] are applied to merge two boost converters with a buck-boost converter. The converter operation and dynamics are represented by a mathematical model. State space analysis along with the small-signal averaging method is performed in each mode of operation to obtain the TFM.

(ii) Tor to determine the controller structure, interaction analysis is carried out to determine the converter's input-output pairing.

(iii) Further, the required performances of the TIID converter are represented using the weight functions W_1, W_2 and W_3 respectively. These are employed to design the robust H_∞ controller.

(iv) The impact of variation of each parameter on dynamics, sensitivity functions, and inverse of weight functions are analyzed and plotted.

The paper is divided into the following sessions: (i) mathematical modeling of the TIID Converter, (ii) quantifying the interactions and identifying i/o pairing to determine the controller structure, (iii) synthesis of the H_∞ controller, (iv) designing of different weight functions, (v) illustrates the impact of variation of each parameter of weight functions on dynamics, sensitivity functions and inverse of weight functions followed by Conclusions.

2 Modeling of TIID Converter

In Figure 1, the converter for TIID is shown. For this integrated converter, three distinct voltage sources (V_{g1}, V_{g2} and V_{g3}) are suggested. Furthermore, for proper load sharing and power continuity, the output voltage V_o and the LVS currents (i_{g1}, i_{g2} are the input currents of V_{g1}, V_{g2}) are regulated. Three duty ratio control signals d_1, d_2 and d_3 are used in the proposed converter to independently regulate each of the three switches. As a result, three different sources of power can supply the load simultaneously or separately. The duty ratios function as the governing inputs of the converter. This enables four different modes of operation to be possible as shown in Figure 2. As a result, each mode of operation's state space equations evaluates the converter's dynamics and performance. The input and output variables are hence functionally dependent on one another. Hence, this functional dependency is modeled by a set of transfer functions assembled in TFM form. To derive the TFM, a state-variable model along with small-signal modeling is implemented in all the operating modes.

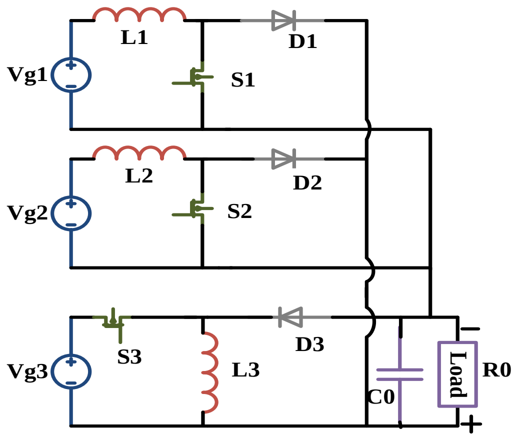

Fig. 1: Circuit diagram of the TIID converter

Eqs (1), and (2) give the state-space equations for the four operational modes, where i =1,2,3,4. The small-signal modeling of the converter can be generated by averaging these state equations as indicated in (3) and applying minor change $\hat{k}$ to each of the state variables as indicated in (4). From there, the TFM G as indicated in (5) is developed in a MATLAB environment. The detailed modeling is given in [23].

$$\dot{x} = A_i x + B_i u \ , \ y = E_{0i}x + F_{0i}u \tag{1}$$

$$y = \begin{bmatrix} v_0 \\ i_{g1} \\ i_{g2} \end{bmatrix} E_{0i} = \begin{bmatrix} E_1 \\ P_{1i} \\ P_{2i} \end{bmatrix} F_{01} = \begin{bmatrix} F_1 \\ F_{1i} \\ F_{2i} \end{bmatrix} \tag{2}$$

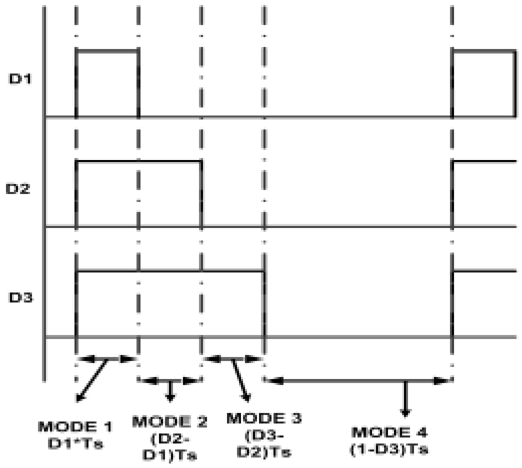

Fig. 2: PWM gating signals for the TIID Converter

$$\begin{bmatrix} A \\ B \\ E \\ F \end{bmatrix} = \begin{bmatrix} d_1A_1 + (d_2 - d_1)A_2 + (d_3 - d_2)A_3 + (1 - d_3)A_4 \\ d_1B_1 + (d_2 - d_1)B_2 + (d_3 - d_2)B_3 + (1 - d_3)B_4 \\ d_1E_1 + (d_2 - d_1)E_2 + (d_3 - d_2)E_3 + (1 - d_3)E_4 \\ d_1F_1 + (d_2 - d_1)F_2 + (d_3 - d_2)F_3 + (1 - d_3)F_4 \end{bmatrix} \tag{3}$$

$$x(t) = X + \hat{x} \ , \ u(t) = U + \hat{u} \ , \ y(t) = Y + \hat{y} \ , d_1 = D_1 + \hat{d}_1 \ ,$$
$$d_2 = D_2 + \hat{d}_2 \ , \ d_3 = D_3 + \hat{d}_3 \ , (1 - d_3) = D^1{}_3 - \hat{d}_3 \tag{4}$$

$$\begin{bmatrix} \hat{v}_0(s) \\ \hat{i}_{g1}(s) \\ \hat{i}_{g2}(s) \end{bmatrix} = \begin{bmatrix} G_{11}(s) & G_{12}(s) & G_{13}(s) \\ G_{21}(s) & G_{22}(s) & G_{23}(s) \\ G_{31}(s) & G_{32}(s) & G_{33}(s) \end{bmatrix} \begin{bmatrix} \hat{d}_1(s) \\ \hat{d}_2(s) \\ \hat{d}_3(s) \end{bmatrix} \tag{5}$$

$$G = \begin{bmatrix} G_{11}(s) & G_{12}(s) & G_{13}(s) \\ G_{21}(s) & G_{22}(s) & G_{23}(s) \\ G_{31}(s) & G_{32}(s) & G_{33}(s) \end{bmatrix} \tag{6}$$

3 Decentralised Controller Structure

Using the TFM G in (6), identify the input-output pairing. It describes which input controls which output predominantly than others. Pairing problem is addressed by performing Interaction Analysis using *RGA* as given in [25]. The TIID converter is designed with the specifications given in Table 1. Using these parameters, the TFM of the TIID converter (6), considering all the modes is obtained in MATLAB and is given from (7)-(15).

Table 1. Specifications and Parameter Values

Parameters	Value
V_{g1}, V_{g2}, V_{g3}	36V,30V,24V
V_o, Load power P_o, R_o	48V, 288W
i_{L1}, i_{L2}	2.5A,2A
L_1, L_2, L_3	150µH, 250µH, 20µH
C_o	200µF
switching frequency f_s	50KHz
Δi_L, ΔV_o	10%, 5%

$$G_{11} = \frac{-0.3488s^4 - 2.493x10^4 s^3 + 1.051x10^9 s^2 + 5.608x10^{12} s + 1.796x10^{15}}{s^4 + 6195s^3 + 6.126x10^7 s^2 + 1.3x10^{11} s + 2.885x10^{13}} \tag{7}$$

$$G_{12} = \frac{0.6379s^4 + 1.293x10^5 s^3 + 6.573x10^9 s^2 + 2.308x10^{12} s + 6.963x10^{13}}{s^4 + 6195s^3 + 6.126x10^7 s^2 + 1.3x10^{11} s + 2.885x10^{13}} \tag{8}$$

$$G_{13} = \frac{-0.4423s^4 - 4.073x10^4 s^3 + 3.755x10^8 s^2 + 2.48x10^{12} s + 8.226x10^{13}}{s^4 + 6195s^3 + 6.126x10^7 s^2 + 1.3x10^{11} s + 2.885x10^{13}} \tag{9}$$

$$G_{21} = \frac{3.249x10^5 s^3 + 2.093x10^9 s^2 + 1.442x10^{13} s + 1.382x10^{16}}{s^4 + 6195s^3 + 6.126x10^7 s^2 + 1.3x10^{11} s + 2.885x10^{13}} \tag{10}$$

$$G_{22} = \frac{-4253s^3 - 7.506x10^8 s^2 - 3.238x10^{13} s - 1.029x10^{16}}{s^4 + 6195s^3 + 6.126x10^7 s^2 + 1.3x10^{11} s + 2.885x10^{13}} \tag{11}$$

$$G_{23} = \frac{2949s^3 + 1.943x10^8 s^2 - 1.899x10^{12} s - 1.215x10^{16}}{s^4 + 6195s^3 + 6.126x10^7 s^2 + 1.3x10^{11} s + 2.885x10^{13}} \tag{12}$$

$$G_{31} = \frac{4.446x10^7 s^2 - 2.665x10^{12} s - 1.243x10^{16}}{s^4 + 6195s^3 + 6.126x10^7 s^2 + 1.3x10^{11} s + 2.885x10^{13}} \tag{13}$$

$$G_{32} = \frac{-2552s^3 - 4.15x10^8 s^2 - 1.577x10^{13} s - 1.4x10^{15}}{s^4 + 6195s^3 + 6.126x10^7 s^2 + 1.3x10^{11} s + 2.885x10^{13}} \tag{14}$$

$$G_{33} = \frac{1.967x10^5 s^3 + 1.237x10^9 s^2 + 1.061x10^{13} s + 1.592x10^{16}}{s^4 + 6195s^3 + 6.126x10^7 s^2 + 1.3x10^{11} s + 2.885x10^{13}} \quad (15)$$

The TIID converter's computed RGA matrix is given in (16). TFM is diagonally dominating, as can be seen from this matrix (0.9505, 0.8920, and 0.9059). As a result, RGA recommends matching the input-output variables of the TIID converter diagonally i.e., $d_1 - V_o$, $d_2 - i_{g1}$ and $d_3 - i_{g2}$. This leads to the decentralized or diagonal controller topology seen in Figure 3. This controller is designed using H_∞ control as described below.

$$RGA(G(s)) = \begin{bmatrix} 0.9505 & 0.0139 & 0.0356 \\ 0.0495 & 0.8920 & 0.0585 \\ 0.0000 & 0.0941 & 0.9059 \end{bmatrix} \quad (16)$$

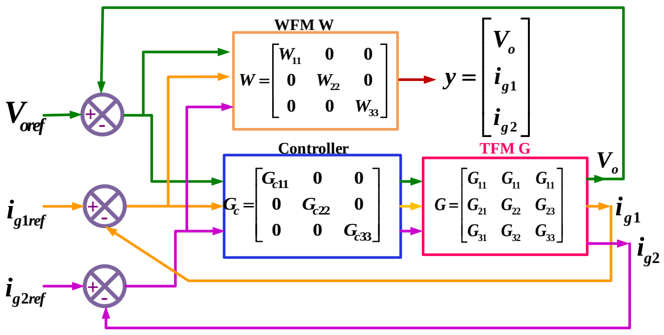

Fig. 3: Schematic of the closed-loop TIID converter

4 Synthesis of Mixed Sensitivity H_∞ Controller

For the TIID converter, any deviation in inputs (V_{g1}, V_{g2}, V_{g3}) and load will reflect in converter dynamics and its characteristics. A robust controller can address this uncertain situation to regulate the three output variables of the TIID converter. The robust controller can be designed by applying loop-shaping along with the H_∞ technique, [26]. This technique allows the designer to shape the frequency response of the converter system and then optimize the response of the system to achieve robustness. Figure 4 shows the LTI model of a system with a plant P and controller K. Equation (17) represents a dynamic model of plant P with its inputs(u, w) and outputs(z, y).

$$\begin{bmatrix} z \\ y \end{bmatrix} = P * \begin{bmatrix} w \\ u \end{bmatrix} \quad (17)$$

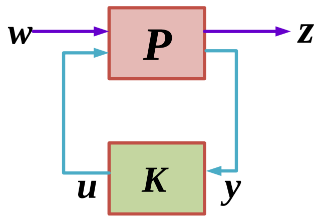

Fig. 4: LTI model of P and K

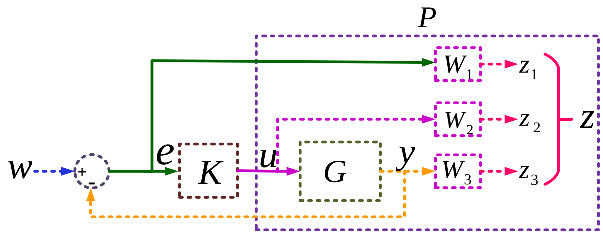

Fig. 5: The augmented plant P with K

To synthesize the controller K for P, the robust controller must reject disturbances and noises injected at the plant output. In H_∞ control, this robustness is acquired by direct loop shaping of singular value plots of a closed loop system. The required performance objectives of the system are represented along with weight functions (loop-shaping filters). The plant performance and robustness can be specified in terms of S and T. S ensures disturbance rejection, KS is the controller effort and T represents tracking and noise attenuation characteristics. Hence, these system performances are represented using the weight functions W_1, W_2 and W_3 respectively. These are incorporated into the system before designing the controller K as shown in Figure 5, where G is the TFM of the converter and W is the Weight Function Matrix (WFM) of W_1, W_2 and W_3. W represents the TFM from w to z as given in equation (18).

In mixed sensitivity H_∞ control method, the controller K which stabilizes the system G is designed such that it minimizes the H_∞ norm of the closed-loop system i.e., $\|W\|_\infty < \gamma$, where $\gamma \le 1$.

$$W(s) = \begin{bmatrix} W_1 S \\ W_2 KS \\ W_3 T \end{bmatrix} \quad (18)$$

5 Designing of Weight Functions

The weight functions W_1, W_2 and W_3 are written in the form of transfer functions that represent frequency response upper bounds for S, KS and T. WFM parameters are selected for this integrated converter using the standard methodology, [27] and these weight functions are designed as follows:

5.1 Design of W_1

To track the reference signal with high accuracy and to subdue the external disturbances, the sensitivity function S should be small enough in the desired frequency range. Choose W_1 large inside the control bandwidth to obtain small $S.W_1$ is a function of desired steady-state error (e_s), Desired bandwidth (ω_s) and Maximum allowed sensitivity peak of the system (M_s) as given in (19).

$$W_1 = \frac{\frac{s}{M_s} + \omega_s}{s + \omega_s e_s} \tag{19}$$

5.2 Design of W_2

W_2 is specified in terms of the desired controller specifications. To limit control effort in a particular frequency band, increase the magnitude of W_2 in this frequency band to obtain small KS. The transfer function of W_2 is given in (20).

$$W_2 = \frac{s + \frac{\omega_{bc}}{M_{bc}}}{e_{bc}s + \omega_{bc}} \tag{20}$$

5.3 Design of W_3

If S is small in the desired bandwidth, then T is large in the desired bandwidth. Therefore, choose W_3 to be large outside the control bandwidth to obtain small T for good robustness and noise attenuation characteristics. The transfer function W_3 is given in (21).

$$W_3 = \frac{s + \frac{\omega_b}{M_b}}{e_b s + \omega_b} \tag{21}$$

The weight function transfer functions given using equations (19- 21) are used for loop shaping to get the desired performance of the closed-loop system thereby designing the controller.

6 Results & Discussion

In this section, the impact of varying the parameters on the dynamics of the system is studied. The parameters of all three weight functions are varied and the impact of each parameter on the dynamics of the system G_{11} are studied. The impact of variation of each parameter on dynamics, sensitivity functions, and inverse of weight functions are analyzed and plotted. Thus, the choice of the parameters is justified and validated from these plots, [28], [29].

To design a controller for G_{11}, the WFM W_{111}, W_{112} and W_{113} of G_{11} are obtained and are given in (22).

$$W_{111} = \frac{0.5s + 100}{s + 20}, W_{112} = \frac{s + 500}{0.01s + 100}, W_{113} = \frac{s + 6667}{0.001s + 10000} \tag{22}$$

6.1 Impact of Parameter Variation of W_{111}

6.1.1 Varying e_s of W_{111}

Consider W_{111}, the parameter e_s is varied from 0.01 to 1 while keeping ω_s and M_s constant. The other two weight functions W_{112} and W_{113} are also kept constant. The variations of dynamics of the step response of the closed loop system of G_{11} are shown in Figure 6, Figure 7, Figure 8 and Figure 9. From Figure 6, it is evident that as e_s is increased the settling time (t_s) decreases implying that a higher value of e_s is suitable for best closed-loop performance. From Figure 7, it is evident that there is no Peak overshoot (P_o) and it doesn't change (NC) with e_s. From Figure 8, it is observed that with an increase in e_s, the steady-state error (e_{ss}) also increases. When $e_s = 0$, the deviation in closed-loop step response is zero. From Figure 9, the Peak magnitude (P_m) decreases with increase in e_s. The step response with varying e_s is given in Figure 10. As e_s increases, the step response deviates indicating the increase in e_{ss}. Thus, from these plots, it can be concluded that a lower value of e_s is suitable to have better closed-loop performance. Similarly, the variation in other parameters and their impacts are studied.

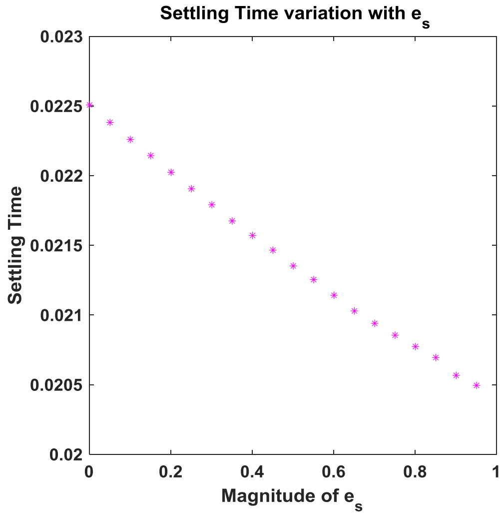

Fig. 6: Variation of t_s with e_s

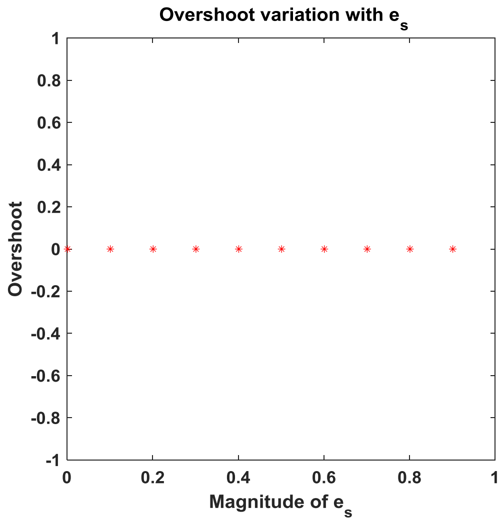

Fig. 7: Variation of P_o with e_s

6.1.2 Arbitrary Variation of Three Parameters on $1/W_{111}$:

The bode plots of $1/W_{111}$ with varying parameters are plotted from Figure 11, Figure 12 and Figure 13. Figure 11, shows that when desired e_s is varied while keeping w_s and M_s constant, the values of gains at low frequency varies (g_{lf}) i.e., when e_s increases g_{lf} also increases while the gain at high frequency(g_{hf}) is constant. In Figure 12, when M_s is varied while keeping e_s and w_s constant, g_{hf} varies i.e., when M_s increases, g_{hf} also increases while g_{lf} is constant. In Figure 13, when w_s is varied while keeping e_s and M_s constant, g_{lf} and g_{hf} are constant but the cross-over frequency (ω_c) varies i.e., with increase in w_s , ω_c is decreased. The Impact of all the parameter variations of WFM on system characteristics is tabulated in Table 2.

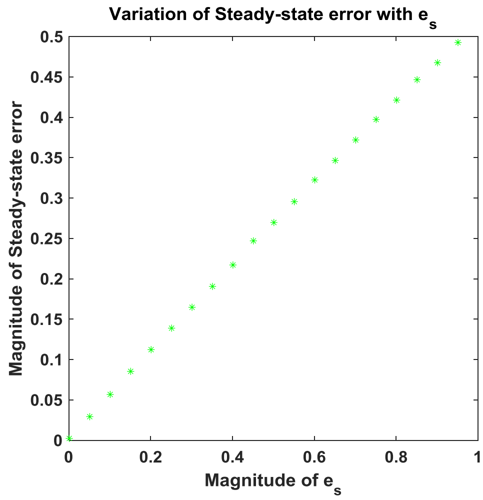

Fig. 8: Variation of e_{ss} with e_s

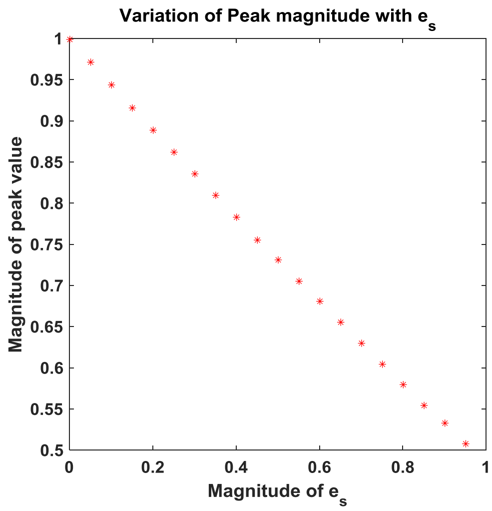

Fig. 9: Variation of P_m with e_s

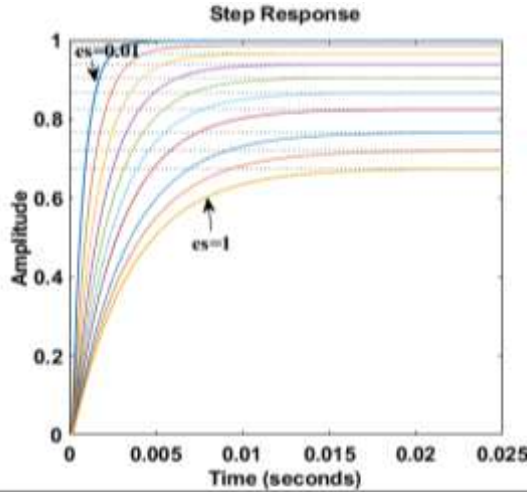

Fig. 10: Variation of Step response with e_s

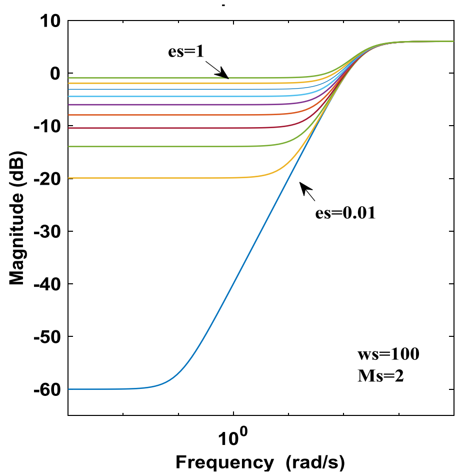

Fig. 11: Bode plot of $1/W_{111}$ with varying e_s.

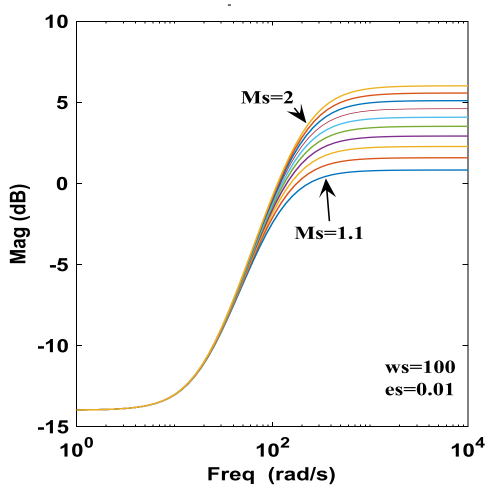

Fig. 12: Bode plot of $1/W_{111}$ with varying M_s

Table 2. Impact of Parameter Variation on System Characteristics

Weight function parameters		Characteristics of Step Response				Remarks on performance characteristics and inverse weight functions	
		t_s	P_o	e_{ss}	P_m		
W_{111}	e_s	↓	none	↑	↓	g_{lf} of S_1 ↑	g_{lf} of $1/W_{111}$ ↑
	ω_s	↓	none	↑	↓	g_{lf} of S_1 ↑	ω_c of $1/W_{111}$ ↓
	M_s	↓	none	↓	↑	g_{lf} of S_1 ↑	g_{hf} of $1/W_{111}$ ↑
W_{112}	e_{bc}	NC	none	NC	NC	NC in KS_1	g_{hf} of $1/W_{112}$ ↑
	ω_{bc}	NC	none	NC	NC	NC in KS_1	ω_c of $1/W_{112}$ ↑
	M_{bc}	NC	none	NC	NC	NC in KS_1	g_{lf} of $1/W_{112}$ ↑
W_{113}	e_b	↑	none	↑	NC	NC in T_1	g_{hf} of $1/W_{113}$ ↑
	ω_b	↑	none	NC	NC	NC in T_1	ω_c of $1/W_{113}$ ↑
	M_b	↓	none	↓	NC	g_{hf} of T_1 ↑	g_{lf} of $1/W_{113}$ ↑

6.2 Simulation Results

The designed Controller with the WFM The test bench is shown in Figure 14, and MATLAB connected with the OPAL4510-RT simulator using RT-LAB simulation software confirms the closed-loop performance of G_c for TIID converter, [27], [28]. The real-time observations are made using a digital storage oscilloscope. Under various operating scenarios, the robust controller's performance is validated.

Fig. 13: OPAL4510-RT Simulator test bench

Figure 14 displays the simulation of the nominal settings given in Table 1. Figure 15 displays the HIL Simulation results of the OP4510 measured in DSO.

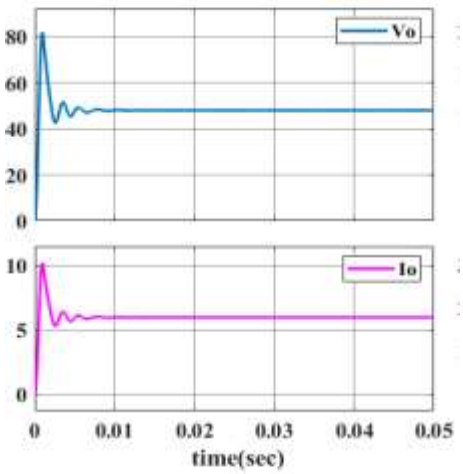

Fig. 14: V_o, I_o of TIID converter

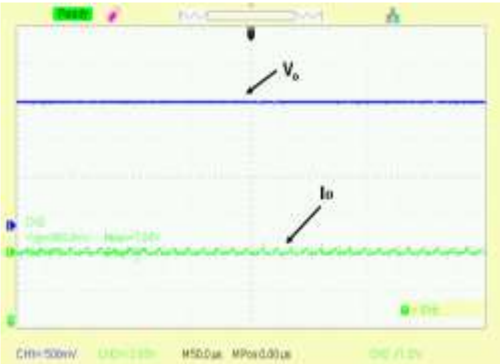

Fig. 15: V_o, I_o of TIID converter

6.2.1 Under Varying Both Load and Sources

In this case, the load and the source voltages are varied and the corresponding V_o and I_o are observed. R_o is varied from 8Ω to 12Ω at t=25msec. At t=40msec, V_{g3} is varied from 24V to 20V. At t=60msec, V_{g2} is varied from 30V to 25V and at t=80msec, V_{g1} is varied from 36V to 30V. The simulation results of the corresponding V_o and I_o are given in Figure 16. Hence, the H_∞ controller can regulate V_o at 48V with variations in load and all the source voltages as shown in Figure 16.

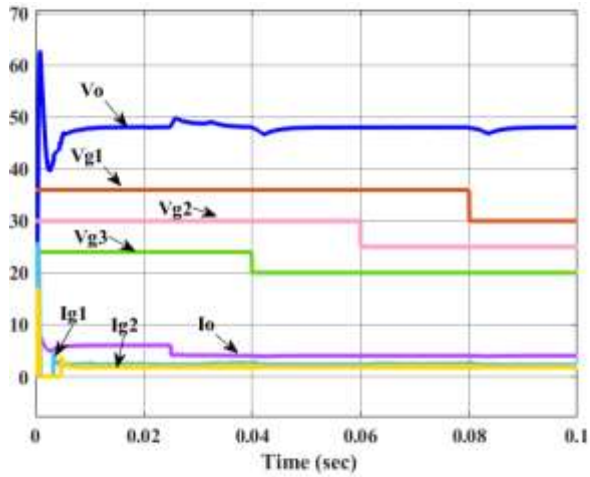

Fig. 16: V_o, I_o of TIID converter with varying load and source voltages

The HIL simulation results using the Data Logger Method (DLM) are given in Figure 17 (a)-(d) and Figure 18 (a)-(d). The HIL simulation results measured in CRO are given in Figure 19, Figure 20, Figure 21, Figure 22 and Figure 23.

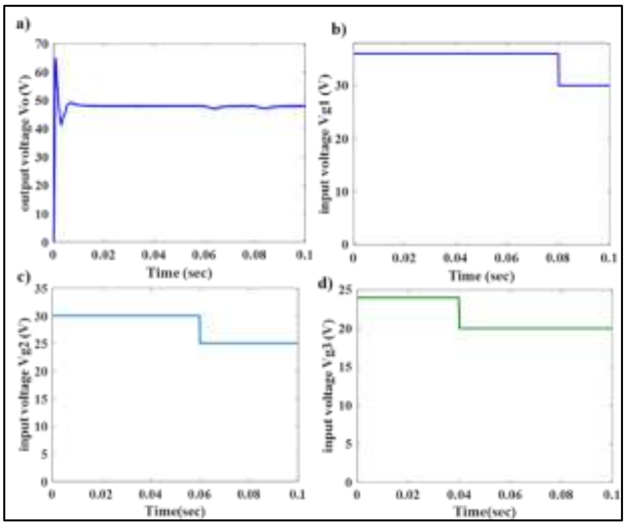

Fig. 17: a) V_o from DLM, b) V_{g1} from DLM, c) V_{g2} from DLM, d) V_{g3} from DLM

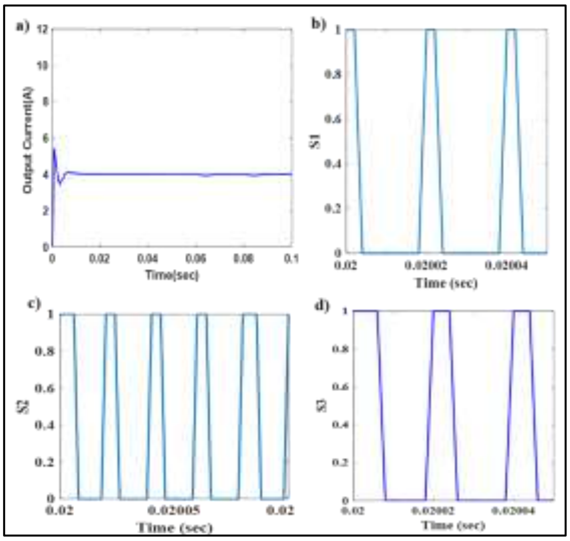

Fig. 18: a) I_o from DLM, b) d_1 of switch S_1 ,c) d_2 of S_2 d) d_3 of S_3 from DLM

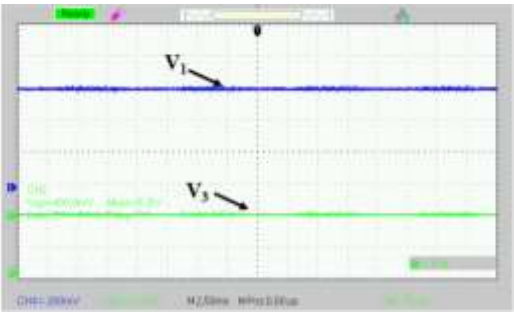

Fig. 19: Input voltage V_{g1} and V_{g3} of TIID converter

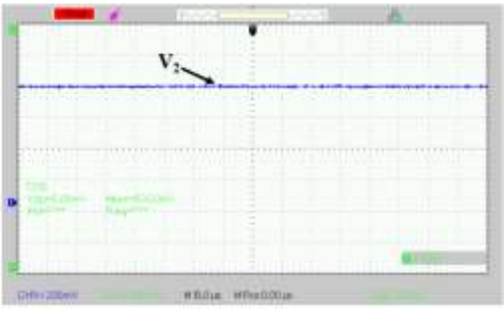

Fig. 20: Input voltage V_{g2} of TIID converter

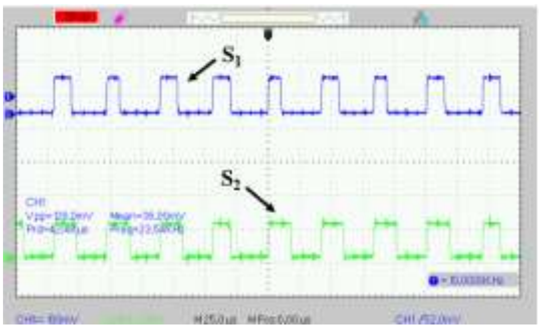

Fig. 21: Duty ratios of S_1 and S_2 of TIID converter

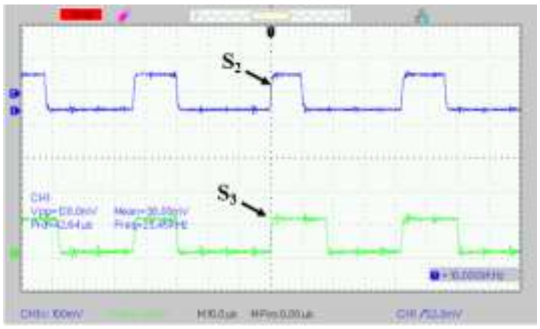

Fig. 22: Duty ratios of S_2 and S_3 of TIID converter

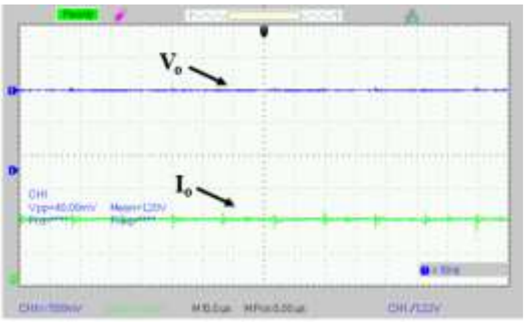

Fig. 23: V_o, I_o of TIID converter

7 Conclusion

The TIID converter is modeled using state-space analysis and a Transfer Function Matrix is acquired from the small signal continuous time model. The desired robustness and the performance of the controller are represented with weight functions (loop-shaping filters). These weight functions are designed using the obtained Transfer Function Matrix. The robustness of the controller depends on the weigh function parameters. The impact of parameter variations of the weight functions on system dynamics and performance is studied and plotted. TIID converter of 288 W, 24V-30V-36V to 48 V is considered and the impact of weight function on closed-loop system dynamics and sensitivity characteristics under varying parameter conditions are analyzed in MATLAB Environment.

The Future scope of this research work is (i) to implement a Dc Microgrid with three different Renewable energy sources as three inputs for the proposed TIID converter of the designed H_∞ controller, (ii) to regulate the output voltage of DC Microgrid with PI controllers, that are to be designed by H_∞ loop-shaping method and (iii) the relation between WFM and Sensitivities at different stages of controller design are to be graphically studied.

References:

[1] X. L. Li, Z. Dong, C. K. Tse and D. D. -C. Lu, "Single-Inductor Multi-Input Multi-Output DC–DC Converter With High Flexibility and Simple Control," in *IEEE Transactions on Power Electronics*, vol. 35, no. 12, pp. 13104-13114, Dec. 2020, 10.1109/TPEL.2020.2991353.

[2] H. Matsuo, W. Lin, F. Kurokawa, T. Shigemizu, and N. Watanabe, "Characteristics of the multiple-input dc-dc converter," *IEEE Transactions on Industrial Electronics*, vol. 51, no. 3, pp. 625–631, Jun. 2004, http://doi.org/10.1109/TIE.2004.825362.

[3] Deepak Agrawal, Rajneesh Kumar Karn, Deepak Verma, Rakeshwri Agrawal, "Modelling and Simulation of Integrated Topology of DC/DC converter for LED Driver Circuit," WSEAS Transactions on Electronics, vol. 11, pp. 18-21, 2020, http://doi.org/10.37394/232017.2020.11.3.

[4] A. Gupta, R. Ayyanar and S. Chakraborty, "Novel Electric Vehicle Traction Architecture With 48 V Battery and Multi-Input, High Conversion Ratio Converter for High and Variable DC-Link Voltage," in *IEEE Open Journal of Vehicular Technology*, vol. 2, pp. 448-470, 2021, 10.1109/OJVT.2021.3132281.

[5] Åström, Karl Johan and Tore Hägglund. "*Advanced PID Control.*" (2005).

[6] M. C. Razali, N. A. Wahab, P. Balaguer, M. F. Rahmat and S. I. Samsudin, "Multivariable PID controllers for dynamic process," *2013 9th Asian Control Conference (ASCC)*, Istanbul, Turkey, 2013, pp. 1-5, https://doi.org/10.1109/ASCC.2013.6606190.

[7] Fredrik Bengtsson, Torsten Wik, "Finding feedforward configurations using gramian based interaction measures", *Modeling, Identification and Control*, Vol. 42, No. 1, 2021, pp. 27-35, http://doi.org/10.4173/mic.2021.1.3.

[8] S. Upadhyaya and M. Veerachary, "Interaction Quantification in Multi-Input Multi-Output Integrated DC-DC Converters," *2021 IEEE 4th International Conference on Computing, Power and Communication Technologies (GUCON)*, Kuala Lumpur, Malaysia, 2021, pp. 1-6, http://doi.org/10.1109/GUCON50781.2021.9573935.

[9] M. Veerachary, "Two-loop controlled buck-SEPIC converter for input source power management," *IEEE Transactions on Industrial Electronics*, vol. 59, no. 11, pp. 4075–4087, Nov. 2012, http://doi.org/10.1109/TIE.2011.2174530.

[10] Michael Green and David J. N. Limebeer. 1994. *Linear robust control*. Prentice-Hall, Inc., USA.

[11] T. Kubo, K. Yubai, D. Yashiro and J. Hirai, "Weight optimization for H∞ loop shaping method using frequency response data for SISO stable plant," *2015 IEEE International Conference on Mechatronics (ICM)*, Nagoya, Japan, 2015, pp. 246-251 https://doi.org/10.1109/ICMECH.2015.7083982.

[12] P. Apkarian, V. Bompart, and D. Noli, "Non-smooth structured control design with application to PID loop-shaping of a process," *International Journal of Robust and Nonlinear Control*, vol. 17, no. 14, pp. 1320–1342, Sep. 2007, http://doi.org/10.1002/rnc.1175.

[13] P. Apkarian and D. Noll, *"The H∞ Control Problem is Solved"*, [Online]. https://hal.science/hal-01653161 (Accessed Date: February 2, 2023).

[14] G. Willmann, D. F. Coutinho, L. F. A. Pereira, and F. B. Líbano, "Multiple-Loop H-Infinity Control Design for Uninterruptible Power Supplies," *IEEE Transactions on Industrial Electronics*, vol. 54, no. 3, pp. 1591–1602, Jun. 2007, https://doi.org/10.1109/TIE.2007.894721.

[15] M. Veerachary, "Two-loop controlled buck-SEPIC converter for input source power management," *IEEE Transactions on Industrial Electronics*, vol. 59, no. 11, pp. 4075–4087, Nov, 2012, http://doi.org/10.1109/TIE.2011.2174530.

[16] K. J Åström, Tore Hägglund, *Advanced PID control. Instrumentation, Systems, and Automation Society*: Research Triangle Park, NC, 2006.

[17] Vilanova, R., & Visioli, A. (2012). PID Control in the Third Millennium. In *Advances*

in industrial control. https://doi.org/10.1007/978-1-4471-2425-2.

[18] Wang, Q. (2008). PID control for multivariable processes. In *Springer eBooks*. https://doi.org/10.1007/978-3-540-78482-1.

[19] T. Kubo, K. Yubai, D. Yashiro and J. Hirai, "Weight optimization for H∞ loop shaping method using frequency response data for SISO stable plant," *2015 IEEE International Conference on Mechatronics (ICM)*, Nagoya, Japan, 2015, pp. 246-251, https://doi.org/10.1109/ICMECH.2015.7083982.

[20] S. D. Tavakoli, S. Fekriasl, E. Prieto-Araujo, J. Beerten and O. Gomis-Bellmunt, "Optimal H∞ Control Design for MMC-Based HVDC Links," in *IEEE Transactions on Power Delivery*, vol. 37, no. 2, pp. 786-797, April 2022, http://doi.org/10.1109/TPWRD.2021.3071211

[21] J. Pérez, S. Cobreces, R. Griñó and F. J. R. Sánchez, "H∞ current controller for input admittance shaping of VSC-based grid applications," in *IEEE Transactions on Power Electronics*, vol. 32, no. 4, pp. 3180-3191, April 2017, http://doi.org/10.1109/TPEL.2016.2574560.

[22] Y. Si, N. Korada, Q. Lei and R. Ayyanar, "A Robust Controller Design Methodology Addressing Challenges Under System Uncertainty," in *IEEE Open Journal of Power Electronics*, vol. 3, pp. 402-418, 2022, http://doi.org/10.1109/OJPEL.2022.3190254.

[23] M. Manogna, B. A. Reddy and K. Padma, "Modeling of a Three-Input Fourth-Order Integrated DC-DC Converter," *2022 International Conference on Smart and Sustainable Technologies in Energy and Power Sectors (SSTEPS)*, Mahendragarh, India, 2022, pp. 83-88,. http://doi.org/10.1109/SSTEPS57475.2022.00032.

[24] Y. C. Liu and Y. M. Chen, "A systematic approach to synthesizing multi-input DC-DC converters," *IEEE Trans Power Electron*, vol. 24, no. 1, pp. 116–127, 2009, http://doi.org/10.1109/TPEL.2008.2009170.

[25] M. Manogna, B. A. Reddy, and K. Padma, "Interaction measures in a three input integrated DC-DC converter," *Engineering Research Express*, vol. 5, no. 1, Mar. 2023, http://doi.org/10.1088/2631-8695/acc0dc.

[26] Sigurd Skogestad and Ian Postlethwaite. 2005. *Multivariable Feedback Control: Analysis and Design*. John Wiley & Sons, Inc., Hoboken, NJ, USA.

[27] K. and J. C. Doyle. Zhou, *Essentials of Robust Control. Upper Saddle River: Prentice-Hall, 1999. ISBN: 978-0135258330*.

[28] Y. Si, N. Korada, Q. Lei and R. Ayyanar, "A Robust Controller Design Methodology Addressing Challenges Under System Uncertainty," in *IEEE Open Journal of Power Electronics*, vol. 3, pp. 402-418, 2022, http://doi.org/10.1109/OJPEL.2022.3190254.

[29] Dulau, M.; Oltean, S.-E. The Effects of Weighting Functions on the Performances of Robust Control Systems. *Proceedings* 2020, *63*, 46. https://doi.org/10.3390/proceedings2020063046.

Contribution of Individual Authors to the Creation of a Scientific Article (Ghostwriting Policy)

The authors equally contributed in the present research, at all stages from the formulation of the problem to the final findings and solution.

Sources of Funding for Research Presented in a Scientific Article or Scientific Article Itself

No funding was received for conducting this study.

Conflict of Interest

The authors have no conflicts of interest to declare.